Title: Tandem Diels-Alder of Dimethylfuran and Ethylene and Dehydration to para-Xylene Catalyzed by Zeotypic Lewis Acids

Authors: Ryan Patet; Wei Fan; Dionisios G Vlachos; Stavros Caratzoulas

To be cited as: 10.1002/cctc.201601584

Link to VoR: https://doi.org/10.1002/cctc.201601584

Tandem Diels-Alder of Dimethylfuran and Ethylene and Dehydration to *para*-Xylene Catalyzed by Zeotypic Lewis Acids

Ryan E. Patet,[1,3] Wei Fan,[2,3] Dionisios G. Vlachos,[1,3] Stavros Caratzoulas[*1,3]

[1]Department of Chemical and Biomolecular Engineering, University of Delaware, Newark, DE 19716
[2]Department of Chemical Engineering, University of Massachusetts Amherst, Amherst, MA 01002.
[3]Catalysis Center for Energy Innovation (CCEI), University of Delaware, Newark, DE

ABSTRACT

The zeotypic Lewis acids Sn-BEA, Zr-BEA and Ti-BEA have recently been reported to catalyze the synthesis of *p*-xylene by dehydrative aromatization of the Diels-Alder product between 2,5-dimethylfuran and ethylene. Although it has been shown that these Lewis acids can catalyze the dehydration of the Diels-Alder cycloadduct, the tandem scheme has precluded decoupling of the two steps needed to infer whether these same catalysts can catalyze the Diels-Alder step. We have employed electronic structure calculations and microkinetic modelling to investigate the Diels-Alder aromatization of 2,5-dimethylfuran and ethylene to *p*-xylene over the Lewis-acidic zeotypes Sn-, Zr- and Ti-BEA. We show that there is only minor catalysis of the Diels-Alder reaction, solely attributable to confinement phenomena varying with the translational freedom allowed to the species inside the zeolite. Microkinetic modelling and sensitivity analysis of the computed rates show that the heterogeneous Diels-Alder pathway does not contribute to the overall rate, and that the homogeneous cycloaddition is rate-limiting at high acid site concentrations. Only the partially hydrolyzed ("open") Lewis acid sites are found to be catalytically active, with moderately Brønsted acidic silanol groups formed that catalyze 2,5-dimethylfuran hydrolysis. Of the Lewis acids tested in this work, Zr-BEA and Sn-BEA have similar activities, in agreement with experiment, while Ti-BEA is found to be inactive, suggesting that the recently reported Ti-BEA activity was likely due to Brønsted acidic defect sites.

Keywords: 2,5-Dimethylfuran, *p*-Xylene, Diels-Alder, Lewis acid, Zeolites, ONIOM, microkinetic modelling

Corresponding Author: cstavros@udel.edu; (302) 831-0362

INTRODUCTION

Across the chemical industry, there is a push to discover new sources for the fuels and chemicals currently derived from fossil resources, and biomass is an ideal feedstock for a number of renewable monomers.[1-10] As inexpensive natural gas liquids (shale gas) are pushing naphtha feedstocks aside, the development of alternative routes for the production of aromatics from renewables is receiving considerable attention.[11-14] Of the possible routes is the dehydrative aromatization of the Diels-Alder (DA) product between bio-based furans with an appropriate dienophile; a tandem scheme where the oxanorbornene derivative obtained from the DA cycloaddition is catalytically dehydrated to an aromatic (Scheme 1). The strategy is showcased by the recently reported formation of *p*-xylene from 2,5-dimethylfuran (DMF) and ethylene over the Brønsted-acidic catalysts H-Y and H-BEA, with yields as high as 90%.[15-18] The same approach was applied by Green *et al.*[19] to convert methylfuran and ethylene to toluene over H-BEA, but the selectivity did not exceed 46%, primarily because methylfuran was lost to side reactions (*e.g.*, alkylation, hydrolysis and oligomerization) (Scheme 1).[19] Independently, Pacheco and Davis achieved Diels-Alder aromatization of ethylene and oxidized variants of HMF over isomorphically substituted Sn-BEA to form terephthalic acid, paving the road for renewable polyterephthalate.[20-22] Orazov and Davis[23] have shown that CIT-6 (Zn-BEA), an easily synthesized zincosilicate analogue of zeolite BEA, can catalyze the Diels-Alder aromatization of ethylene and methyl 5-(methoxymethyl)-furoate to form methyl 4-(methoxymethyl)-benzoate, and that of ethylene and the dimethyl ester of 2,5-furandicarboxylic acid to form dimethyl terephthalate.[23] The work of Pacheco and Davis prompted Chang *et al.*[24] to investigate the Diels-Alder aromatization of DMF and ethylene to *p*-xylene over the Lewis-acidic zeotypes Sn-, Zr- and Ti-BEA. Remarkably, they found that these catalysts are just as effective as H-BEA in influencing the rate of the tandem scheme, while reducing the hydrolysis of DMF.[25] Among the tested catalysts, Zr-BEA exhibited superior performance with 80% selectivity to *p*-xylene at 80% conversion of DMF. Sn-, Ti-, and H-BEA, however, deactivated noticeably faster, and only achieved about 60% DMF conversion, with lower selectivity to *p*-xylene. The lower yields notwithstanding, the zeotypic Lewis acids exhibited longer lifetimes than H-BEA, attributed to low selectivity to the DMF hydrolysis product, 2,5-hexandione (which can oligomerize) and to low coke formation.

However, because of the fleeting existence of the cycloadduct in all these studies, kinetics experiments have not been able to decouple the two steps and thus elucidate whether these Brønsted- and Lewis-acidic zeotypes have any effect on the rate of the Diels-Alder step itself. With furans being among the less reactive dienes, overcoming the challenge of accelerating the cycloaddition reaction will be a pivotal step in the success of producing aromatics by Diels-Ader aromatization of biomass-derived furans and appropriate dienophiles.

Brønsted and Lewis acids are known to accelerate a variety of DA reactions.[26] The mechanism by which they influence the rate of the DA reaction can readily be explained in terms of the frontier molecular orbital (FMO) theory.[27-33] In normal electron demand, protonation or complexation with the Lewis acid of the dienophile lowers the energy of its LUMO and closes the gap to the HOMO of the diene, increasing the interaction between the two FMOs and thus the rate of the reaction. In recent years, Diels-Alder reactivity has also been rationalized in terms of the polar character of the transition state and of the concepts of electronic hardness and electrophilicity.[34-42]

Calculations by Nikbin *et al.*[15, 25, 43] and by Patet *et al.*[18] have asserted that neither Brønsted nor alkali-exchanged Lewis acid zeotypes can influence the rate of the DA between DMF and ethylene. Brønsted-acidic zeolites, such as H-BEA or H-Y, cannot do so for a couple of reasons. First, DMF binds more strongly to the active site than ethylene. Second, the proton has higher affinity for the α-position of the

furan ring instead of the O-heteroatom and thus protonation breaks the requisite orbital symmetry. A similar situation has been observed in alkali-exchanged zeolites, where calculations have shown that the preferred coordination of DMF to the active site *does* lower the LUMO of the furan, but not enough to activate the inverse electron demand mode and to compensate for the deactivation of the normal electron demand mode due to the concomitant lowering of the HOMO of DMF.[25, 43, 44] So, over alkali-exchanged zeolites, the reaction follows bi-directional electron demand (namely, both HOMO(diene)-LUMO(dienophile) and HOMO(dienophile)-LUMO(diene) driven[30]) with no noticeable acceleration. Although inverse electron demand cycloadditions have been reported, strong Lewis acids are required.[38, 45, 46] Alkali cations such as Li^+ and Na^+, with a large positive surface charge density, should in principle be effective Lewis acid catalysts,[25, 44, 47] but when they are embedded in zeolitic frameworks, charge screening by surrounding framework oxygen atoms diminishes their catalytic activity.[43]

It is an open question, however, whether the framework substituted zeolites tested by Chang *et al*.[24] can catalyze the Diels-Alder between DMF and ethylene. Given the importance of the Diels-Alder cycloaddition as a tool in synthetic organic chemistry and, in particular, its significance for the development of a technology for the sustainable conversion of furans to aromatics, in this article we use electronic structure calculations and microkinetic modelling to study the Diels-Alder aromatization of DMF and ethylene in Sn-, Zr-, and Ti-BEA and to assess their ability to catalyze Diels-Alder cycloaddition.

METHODS

Electronic structure calculations. In all the calculations the zeolite was modelled as a mechanically embedded three-layer (QM/QM/MM) ONIOM cluster model.[48-50] To build the model, a metal-atom (Sn/Ti/Zr) is substituted for a Si-atom in the T9 position of the BEA unit cell[51] and then a cluster is hewn out of the crystal by selecting the atoms in the first five tetrahedral coordination spheres surrounding the metal-atom. All dangling bonds are saturated with H-atoms for a model containing 118 tetrahedral atoms (118T) and a stoichiometry of $[Sn/Ti/Zr]Si_{117}O_{180}H_{112}$ (shown in Figure S1 of the Supporting Information). The small layer (17T) is allowed to relax and is treated at the M06-2X/6-311G(2df,p) theory level, with the metal atoms modelled with the LANL2DZ effective core potential.[52] All reactants, intermediates, and products are treated as part of this small layer. The intermediate layer (17T) is treated at the M06-2X/6-31G(d,p)//M06-2X/3-21G theory level and is frozen geometrically to maintain the zeolite pore structure integrity. The real layer (84T) is treated with the universal force field (UFF) molecular mechanics theory,[53] and is also frozen geometrically. Relaxing the intermediate- and low-level layers led to spurious imaginary frequencies in certain calculations.

Both unhydrolyzed ("closed"), metal-$(OSi)_4$), and partially hydrolyzed ("open"), ((HO-metal-$(OSi)_3$), active sites are considered, as shown in Figures 1(a) and 1(b).[54] Only closed sites of Ti-BEA are considered, as Ti-BEA is not thought to form open sites.[55]

Solution phase calculations were performed using the SMD model[56] of heptane. Ground and transition states were characterized by frequency analysis and all transition states were further validated by intrinsic reaction coordinate (IRC) calculations.[57] The thermal corrections to the electronic energies were computed using the q-RRHO (quasi-rigid rotor harmonic oscillator) approximation of Grimme[58] and of Head-Gordon.[59]

More details on the development and benchmarking of the methodology can be found in our recent publication.[60] We should note that we have also performed single-point energy calculations at the M06-

2X/Def2TZVP theory level for the small (high-level ONIOM) layer without a significant effect on the calculated free energy profiles (Table S1 of the Supporting Information).

Natural population analysis (NPA) was performed with the NBO 6.0 software suite.[61] Bader analysis,[62] was performed using the AIM2000 program. The NBO and Bader analyses were performed on the isolated ONIOM small layer (capped with H atoms and frozen in the geometry of the fully optimized ONIOM model).

Microkinetic Modelling. A microkinetic model (MKM) has been constructed and parameterized based on the free energy profiles obtained from the electronic structure calculations. The reaction network includes the following pathways: homogeneous and heterogeneous Diels-Alder cycloaddition of DMF and ethylene; homogeneous and heterogeneous dehydration of the Diels-Alder product; heterogeneous hydrolysis of DMF; and the adsorption/desorption of all reactants, products, and stable intermediates onto and from the active site. For the open sites, we have allowed for two distinct catalytic pathways: the Lewis acidic metal site pathway and the Brønsted acidic pathway that involves the Si-OH group in the immediate vicinity of the metal site. For the closed active sites, only coordination to the metal site is considered.

RESULTS

Characterization of the active site. In Table 1, we show geometrical parameters of the active site and the NPA charges of its atoms. The metal-framework oxygen bonds are longer that the Si-O bonds they are replacing, in the 1.8-1.9 Å range commensurately with the relative atomic size from ~1.6 Å for Si to for the metal substituents. This difference in atomic size causes a change in the local zeolite framework structure, as evidenced by the T-O-Si bond angle (where T represents Sn, Ti, or Zr), with the smallest substituent, Ti, resulting in the broadest angle of ~138° and to the largest, Zr, having a sharper angle of ~132°. A difference can be seen in the atomic charges of the incorporated metal atoms. The Sn and Zr atoms are more positively charged (+2.8 and +2.5) than Ti (+1.9). The change in structure from the closed to the open sites does not significantly change either the bond distances or atomic charges of these systems, although a change in the local structure is evident from a decrease in the T-O-Si angle to ~100°.

The Si-OH group of the open active site is moderately Brønsted acidic. The NPA charge of the H-atom is ~+0.5 for all the zeotypic Lewis acids considered; and is also the same as the partial change of the Brønsted-acidic hydrogen atom of Al-BEA. However, the computed deprotonation energies (DPE) (see. Eq. 1) show a dependence on the metal atom. In the case of Zr-BEA the DPE is ~300 kcal/mol whereas for Sn-BEA it is ~285 kcal/mol, meaning that the latter has somewhat stronger Brønsted-acidic character. For perspective, the DPE of Al-BEA is 271.1 kcal/mol.

$$DPE = E_{Z-H} - E_{z^-} - E_{H^+}. \quad (1)$$

Catalysis of the Diels-Alder and dehydration reactions. The mechanism for the formation of *p*-xylene and water from DMF and ethylene is shown in Scheme 2, whereby the oxanorbornene intermediate formed by Diels-Alder cycloaddition subsequently undergoes dehydration in three steps to form *p*-xylene.[15, 18, 25, 43] Enthalpy profiles for the closed active sites are shown in Figure 2(a) and for the open active sites in Figure 2(b).

For the uncatalyzed Diels-Alder reaction in heptane, the reaction barrier is 24 kcal/mol at the M06-2X/6-311G(2df,p) theory level. A more accurate calculation of the uncatalyzed reaction at the CBS-QB3 theory level yields an enthalpy barrier of 20 kcal/mol. For all the catalysts considered, the Diels-Alder

transition state is stabilized by 20-25 kcal/mol relative to the gas phase, depending on the active site metal center and on whether the site is hydrolyzed or not. We also see similar stabilization of the interacting complex of the two addends, with preferential coordination of the furan to the active site. Relative to the gas phase, the interactive complex is stabilized by *ca*. 20 kcal/mol on the catalysts with closed active sites (Figure 2(a)) and by *ca*. 20-25 kcal/mol on those with open sites (Figure 2(b)). As a result, the intrinsic DA enthalpy barriers, *viz*. relative to the active-site-coordinated interacting complex, remain in the 23-25 kcal/mol range—the same as in the uncatalyzed reaction. Thus, with the furan coordinated to the active site, the Lewis acid centers seem unable to induce sufficient charge transfer to promote inverse electron demand cycloaddition. We will later see that confinement and entropic phenomena may be more consequential to the adsorption and stability of the reactants and transition state complexes, and thereby to the Diels-Alder of furans with alkenes not bearing electron withdrawing groups.

In the absence of catalyst, the enthalpy of activation of the dehydration of the oxanorbornene derivative is 60 kcal/mol and is associated with the breaking of the C-O bridge. When the reaction is carried out in Sn-, Zr-, or Ti-BEA with unhydrolyzed active sites, the respective barriers decrease to 31, 30, and 36 kcal/mol, respectively. These energy barriers seem to track the partial charges of the metal centers, with Ti being the less positively charged of the three. In Sn- and Zr-BEA with hydrolyzed active sites we can have coordination of the cycloadduct either to the Lewis-acidic metal center or to the moderately Brønsted-acidic silanol group. In the former case, the C-O cleavage intrinsic barriers drop further to 25 and 24 kcal/mol for Sn- and Zr-BEA, respectively, and the reaction proceeds through the formation of an alkoxy intermediate species. Figures 3(a) and 3(b) show the coordination geometries of the cycloadduct to the metal center of the closed and open sites of Sn-BEA, respectively. We see that they are very similar, other than the distance between the O atom of the cycloadduct and the Sn atom being 0.5 Å shorter at the open active site. As a result, the cycloadduct and the alkoxy intermediate that result from the opening of the C-O bridge bind more strongly to the open site than the closed one, by 10-15 kcal/mol. Although the partial charges of the metal centers seem to track the relative activities of Sn-, Zr- and Ti-BEA, they still cannot explain the differences in activity between the closed and open sites, as the hydrolysis of the closed sites has no effect on the population of the metal orbitals.

When the cycloadduct coordinates to the silanol group of an open site, the breaking of the C-O bridge is accompanied by proton transfer from the silanol to the O atom of the bridge, evoking enforced general acid catalysis. However, the resulting protonated intermediate is very unstable relative to the alkoxy intermediate mentioned earlier. The corresponding intrinsic enthalpy barriers are respectively 29 and 30 kcal/mol for Sn- and Zr-BEA with open sites. These are practically the same as those found for the closed active sites and about 5 kcal/mol higher than the corresponding barriers across the pathways involving coordination to the Lewis acid center alone.

To better understand the acid strength of these solid acids and their effect on the oxanorbornene C-O bond, we have analyzed the electron density and the Laplacian of the electron density of the coordinated cycloadduct using Bader's theory. In Figure 4, we plot the values of the density and of its Laplacian at the bond critical point (BCP) of the C-O bond. The density at the BCP correlates well with the cleavage barrier. Adsorption onto the open active sites results in a greater depletion of the C-O bond density than to the closed active site, and thus a lower cleavage barrier. The negative of the Laplacian is indicating a concentration of charge at the BCP representative of a covalent-type bond[62] and demonstrates a similar linear trend.

Confinement and entropy. Confinement and the concomitant entropic changes can influence the Gibbs free energy changes along a catalytic pathway. Upon adsorption, it is unknown how much freedom

a guest molecule has to move inside the pore. We have considered both immobile and mobile adsorbates. In the latter case, in particular, any one of the guest molecules has been allowed to move freely in either one or two dimensions; and for the calculation of the corresponding translational entropy we have assumed either a length of 800 pm or a molecular surface area of 800x800 pm^2, characteristic of the BEA framework pore size.[63]

Calculated free energy profiles of the cycloaddition are shown in Figure 5 for Sn, Zr and Ti, both for closed and open sites; profiles for the entire tandem scheme are shown in Figures S2, S3, and S4 of the Supporting Information. The assumption of immobile adsorbates (Figure 5(a)) leads to the largest entropic losses and neither DMF nor the DMF-ethylene interacting complex adsorb favorably in the zeolite. In this case one should expect very low DMF coverages. The DA apparent free energy barriers, $\Delta G^{\ddagger}$, are in the range of 41-46 kcal/mol, namely 0-5 kcal/mol higher than the uncatalyzed reaction in heptane ($\Delta G^{\ddagger}$=41 kcal/mol at 250°C). For mobile adsorbates with one translational degree of freedom in the pore (1D), DMF binds only to the open-Sn- and open-Zr active sites, albeit weakly, whereas the complex of the two addends is unstable in all zeolites tested (Figure 5(b)). In the 1D case, the apparent Gibbs free energy of DA activation is *ca*. 36 kcal/mol for open-Zr, 38 kcal/mol for open-Sn, and *ca*. 40 kcal/mol for the rest. Therefore, we see a 1-5 kcal/mol acceleration, at the most. Allowing for two translational degrees of freedom in the pore (2D) predicts stronger DMF binding in all the systems Figure 5(c). However, the DMF-ethylene complex remains unstable, although less so in open-Sn and open-Zr. In the 2D case, the Gibbs free energies of activation are in the range of 36-38 kcal/mol, namely a 3-5 kcal/mol drop relative to the uncatalyzed reaction. In the above discussion, the apparent activation energies are transition states referenced to either isolated reactants or adsorbed DMF, whichever lies lower.[64-66] To see this, one should consider the rate expression $v_{DA} = k_{DA}K_{DMF}K_{eth}[DMF][eth]C_0/(1 + K_{DMF}[DMF])$, which describes the rate along the heterogeneous DA pathway for unstable DMF-ethylene interacting complexes, a good approximation according to the free energy profiles of Figure 5. In this expression, k_{DA} is the intrinsic DA rate constant on the catalyst, K_{DMF} is the DMF adsorption equilibrium constant, K_{eth} is the equilibrium constant for the formation of the ethylene-DMF-active site complex that follows DMF adsorption, and C_0 is the concentration of active sites. For unfavorable DMF binding, one can further simplify to $v_{DA} \cong k_{DA}K_{DMF}K_{eth}[DMF][eth]C_0$ because $K_{DMF}[DMF] \ll 1$, whereas for favorable DMF binding $K_{DMF}[DMF] \gg 1$ and $v_{DA} \cong k_{DA}K_{eth}[eth]C_0$.

Thus, depending on the entropic losses, the free energy profiles suggest transition from no catalysis of the Diels-Alder for immobile adsorbates in the pore, to modest catalysis in the 1D (only Zr and Sn) or 2D cases by *ca*. 1-5 kcal/mol. We should note that the latter two cases do not seem in line with the nonlinear behavior of the rate of the tandem scheme as a function of the acid site concentration. Chang *et al*.[24] have reported that the rate varies linearly at small acid site concentrations and that it reaches a plateau at high ones, suggesting a switch in the rate-limiting pathway—to one that is unaffected by the presence of a catalyst. For a more complete picture of the overall kinetics and of the various contributions to the overall rate, we have employed microkinetic modelling and investigated all three cases of adsorbate mobility. We compare the predicted *p*-xylene formation rates with experimental data[24] and obtain apparent activation energies at four different catalyst loadings, which we compare with experimental values obtained by Yu *et al*.[67]

Hydrolysis of 2,5-dimethylfuran. Before we delve into the micro-kinetic model, however, we shall digress to discuss briefly the most dominant, undesired side-reaction: the hydrolysis of DMF to 2,5-hexanedione, shown in Scheme 3. Experimentally, 2,5-hexanedione is observed in the products, demonstrating that Sn-, Zr- and Ti-BEA do not completely eliminate it. Water for this reaction can either

be found residually in the experimental system, or is produced through the dehydration of oxanorbornene. Brønsted acids catalyze the hydrolysis by protonating the β-C of DMF, before a water molecule nucleophilically attacks the α-C.[68] Such an acidic proton, however, is not available in the zeotypic Lewis acids with unhydrolyzed active sites, and our calculations have yielded barriers of 51 kcal/mol, suggesting no catalysis by the Lewis-acidic metal center. In fact, catalysis of the hydrolysis is possible only at open active sites *and only with the involvement* of the modestly Brønsted-acidic Si-OH group, requiring a barrier of about 35 kcal/mol. So, the presence of 2,5-hexedione among the products indicates, albeit indirectly, the presence of open active sites or of defect sites.

Microkinetic modelling. Given the error inherent in electronic structure calculations of systems so complex as ours, our intent in employing microkinetic modelling is not so much to test the ability of different functionals to predict the kinetics as to interpret the experimental data using the best available estimates of the relevant kinetic parameters, in order to predict rates that match the experimental ones as closely as possible. We have run the microkinetic model for two sets of kinetic parameters that differ in the theory level used to model the homogeneous Diels-Alder reaction. In the first set, the kinetics of the homogeneous DA was treated at the M06-2X/6-311G(2df,p) level, *viz*., at the same level as the high-theory layer of the ONIOM model. In the second set, the homogeneous DA was treated at the CBS-QB3 level. In the latter, the thermodynamic consistency of the microkinetic model was ensured by adjusting the cycloadduct adsorption/desorption equilibrium constant—a fast step that has no effect on the overall reaction rate (Tables S2 and S3 of the SI). Of the two sets of parameters, the first (M06-2X/6-311G(2df,p)) underestimates the rate of *p*-xylene formation by a factor of 10, whereas the second overestimates the rate by only a factor of 2, matching the experimental data much closer. In the following, we present and discuss results obtained from the latter. The kinetic analyses based on the first set of parameters is presented in the Supporting Information, Tables S4 and S5, and Figures S5 and S6. We should stress that both sets of parameters lead to the same qualitative conclusions, the differences in the predicted rates notwithstanding.

In Figure 6, we plot the *p*-xylene production rate against the acid site concentration. When the adsorbates are treated as immobile (Figure 6(a)), only open-Sn-BEA and open-Zr-BEA show activity. Sn-BEA is also predicted to be less active than Zr-BEA and does not reach a plateau over the range of acid site concentrations considered, for reasons that become clear from sensitivity analysis of the rate (*vide infra*). In Zr-BEA, the rate increases up to an acid site concentration of ~2 mM, before plateauing at a rate of ~500 mM/h, which is in satisfactory agreement with the experimental value[24] of ~200 mM/h, considering that at 250°C a factor of two can be traced to a free energy error of about 1 kcal/mol. When we assume mobile species with one or two translational degrees of freedom (Figures 6(b) and 6(c)), the activity of open-Sn-BEA becomes comparable to that of open-Zr; we also see clear plateauing of the rate at high acid site concentrations, in contrast to immobile adsorbates. Quite interestingly, we see increased closed-Zr-BEA activity if we allow for adsorbate mobility, but still less than open-Zr and open-Sn. The rest of the tested catalytic systems, closed-Sn, and closed-Ti, are inactive on account of the significantly higher dehydration barriers, irrespective of adsorbate mobility (Figures S2, S3, and S4 in the SI). Sensitivity analysis of the computed rates (Figure 7), in conjunction with the free energy profiles, can help us apprehend the reasons behind the rate behavior. The sensitivity analysis for the five active systems (open-Sn and open-Zr and closed-Zr, with immobile or mobile adsorbates) at four acid site concentrations, 0.1, 1, 5 and 12 mM, reveals that at small acid concentrations the rate-limiting step is the dehydration of the cycloadduct, presumably because there are not enough active sites to bind and turn the homogeneously produced cycloadduct into *p*-xylene, despite the fact that the heterogeneous dehydration

requires much less activation than the homogeneous DA, according to the computed energy profiles. This is in line with the linear behavior seen in Figure 6 and with earlier studies of the reaction on Brønsted acidic zeolites. At high acid concentrations, the rate is not limited by the availability of active sites but rather by how fast cycloadduct can be produced homogeneously. Thereby, the rate approaches a maximum, which for the most part is determined by the homogeneous Diels-Alder, invariably for all the catalytic models tested. Quite remarkably, the heterogeneous DA pathway makes almost no contribution to the rate, as the corresponding normalized sensitivity coefficients (NSC) are less than 0.01 (not shown in Figure 7). Comparing Figures 7(a) and 7(d), respectively for open-Sn and open-Zr with immobile adsorbates, we see that in open-Sn the heterogeneous dehydration pathway contributions to the rate (green and red bars) are substantial even at 12 mM, which explains why the rate reaches its maximum value slower than in open-Zr. In open-Sn with mobile adsorbates (Figures 7(b) and 7(c)), on the other hand, the contribution of the dehydration pathway is substantially diminished at concentrations higher than 5 mM and thereby we see activity very close to that of open-Zr, at all acid concentrations. These results are in agreement with experiment, and qualitatively independent of the theoretical model used for the parameterization of the homogeneous Diels-Alder reaction (cf. Figure 7 and Figure S6 in the SI). Closed-Zr is more active than the rest of the closed-active-site systems because of faster dehydration. In the best case scenario for all catalysts tested—translational entropy of adsorbates in two dimensions—the cycloadduct bridge C-O cleavage free energy barrier is *ca*. 27 kcal/mol in closed-Zr, compared with *ca*. 36 kcal/mol in closed-Sn and 40 kcal/mol in closed-Ti. Yet, this barrier is still higher than those in open-Sn and open-Zr, around 20 kcal/mol in both (Figures S2, S3, and S4 in the SI). As a result, the rate of *p*-xylene formation is determined by the dehydration reaction even at acid site concentrations as high as 12 mM (Figures 7(g), 7(h) and 7(i)), without reaching a plateau.

In Figure 8, we plot the DMF conversion over time. For the zeolitic Lewis acids that were deemed inactive, it is clear that the lack of activity arises from failure to convert DMF and is not due to undesired products, e.g., 2,5-hexanedione. When adsorbates are treated as immobile (Figure 8(a)), the DMF conversion over time is in very good agreement with experiment for open-Sn and open-Zr. When mobile adsorbates are considered (Figures 8(b) and 8(c)), we see an increase in the DMF conversion in closed-site Zr-BEA, which is consistent with the rate increase observed in Figures 6(b) and 6(c).

In Figure 9, we plot the product formation as a function of DMF conversion in open-Sn-BEA and open-Zr-BEA. Both immobile and mobile adsorbates produced the same results. For open-Sn, (Figure 9(a)), there is satisfactory agreement for both the *p*-xylene and 2,5-hexanedione yields. At ~60% DMF conversion, the 2,5-hexanedione yield reaches a maximum before beginning to decrease, as the model shows that equilibrium converts it back to DMF as the latter is consumed. The comparison of open-Zr (Figure 9(b)) is also in satisfactory agreement with experiments. The 2,5-hexanedione production is predicted to be lower than in Sn-BEA, in qualitative agreement with experiments, and does not reach its maximum until ~90% conversion of DMF.

Using the MKM, we have also obtained apparent activation energies at four different acid site concentrations (0.1, 1.0, 5.0 and 12.0 mM). In Table 2, we compare the computed apparent activation with the experimental ones obtained by Yu *et al*.[67] For the Lewis acids that showed the greatest activity (open active sites), the apparent activation energies at low acid site concentrations are in the 13-17 kcal/mol range before increasing to ~21 kcal/mol as the catalyst loading increases. This increase in apparent activation energy is in line with the predicted change in rate-determining step, from the fast heterogeneous dehydration at low acid concentrations to the relatively slow, uncatalyzed homogeneous Diels-Alder cycloaddition at high acid concentrations. The closed-Zr, which showed lower activity than

either of the systems with open active sites, shows the opposite trend, namely a decrease in apparent activation energy, from *ca*. 20 to 17 kcal/mol as the acid site concentration increases. The sensitivity analysis for closed-Zr indicates that both homogeneous Diels-Alder cycloaddition and heterogeneous dehydration are active pathways at the higher catalyst loading, suggesting that a single pathway cannot explain the observed barrier. The agreement with experiment is overall quite satisfactory. More specifically, the experimental values of 15.5 and 16.3 kcal/mol for open-Sn and open-Zr, respectively, are in good agreement with the computed values at low acid site concentrations and they also indicate that the reactor was operated in the dehydration-limited regime.[67]

DISCUSSION

The computed enthalpy profiles do not suggest catalysis of the Diels-Alder of DMF and ethylene since the barriers are consistently in the 23-25 kcal/mol range, compared to the 24 kcal/mol barrier of the unanalyzed reaction in heptane solvent. Thus, from an electronic point of view, the Lewis acid centers seem unable to induce sufficient charge transfer to promote inverse electron demand cycloaddition when the furan is coordinated to the active site. Confinement and the attendant entropic phenomena turn out to have a modest effect on the Diels-Alder reaction. For immobile adsorbates, the free energy profile barriers indicate no catalysis by either one of the zeotypic Lewis acids tested in this work. If we allow for adsorbates with one or two translational degrees of freedom, then the Diels-Alder apparent free energies drop by 1-5 kcal/mol relative to the uncatalyzed reaction. Although we have no way of ascertaining the translational freedom of the DA addends in the pores, this modest decrease suggests minor catalysis, which should be solely attributed to entropic effects. Notwithstanding this uncertainty, the microkinetic model and the accompanying sensitivity analyses reveal unequivocally that the heterogeneous DA pathway has negligible contribution to the overall rate of the tandem Diels-Alder aromatization. Only the homogeneous DA pathway controls the rate of the reaction, and then only at high acid site concentrations. Comparing the rates of the homogeneous and heterogeneous DA reactions, we see that, depending on the system, the latter is slower by 3-7 orders of magnitude when compared to the homogeneous reaction at the CBS-QB3 level (Table S6) or 2-6 orders of magnitude when compared to the homogeneous reaction at the M06-2X/6-311G(2df,p) level (Table S7)—the combined effect of the modest drop in activation energy, the rather weak binding of DMF in some systems, and the unstable nature of the interacting complex of the two addends due to entropic losses.

If we consider the CBS-QB3 parameterization of the homogeneous DA reaction, the above order of magnitude differences suggest that, even for the best case scenarios, an *additional* decrease in the heterogeneous DA activation energy by *at least* 8 kcal/mol would be required before it became catalytically relevant. For example, in the cases of open-Sn, open-Zr and closed Zr, the heterogeneous DA activation energies would have to be further reduced by *ca*. 12, 14 and 14 kcal/mol, respectively, at 12 mM catalyst loading. These figures should be reduced by 4 kcal/mol if we consider the M06-2X/6-311G(2df,p) parameterization of the homogeneous DA, since at this theory level the homogeneous DA reaction is predicted to be slower by that amount compared with CBS-QB3.

Our calculations show that the open sites are catalytically more active than the closed ones. Although there is the potential for Brønsted acidity within the zeolites with open sites (from the formation of silanol groups), the calculations predict higher activity by the Lewis-acidic metal centers – especially for Zr-BEA. This is important for two reasons. First, the quite remarkable finding that Lewis acids can catalyze dehydration reactions opens the possibility of a wider range of catalysts, beyond Brønsted acids, capable of catalyzing the dehydrative aromatization of Diels-Alder products between functionalized furans and

olefins. Second, we show for the first time that the silanol groups of the open sites can effect Brønsted acid catalysis, and are in fact solely responsible for the hydrolysis of furans. Thus, elimination of undesired side-reactions that require Brønsted acid catalysis, including side reactions that can cause catalyst coking, might require the design of catalysts that do not possess Brønsted acidity.

Finally, and in stark contrast to what Chang *et al*. have reported,[24] our calculations predict that Ti-BEA (with unhydrolyzed Lewis acid sites) is a very weak Lewis acid and practically inactive (Figure 6), as we found no catalysis of the dehydration of the Diels-Alder cycloadduct. (As we noted earlier, our conclusions hold irrespective of the theory level used in the small (high-level) layer. Single-point energy calculations at the M06-2X/Def2TZVP theory level for the small layer on pre-optimized structures did not show a significant effect on the calculated free energy profiles (see Table S1 of the Supporting Information)). We believe that this strongly suggests the presence of Brønsted-acidic defect sites in the Ti-BEA tested by Chang *et al*. Our finding is in agreement with a recent report by Pacheco *et al*.,[20] who found that the Diels-Alder aromatization of methyl 5-(methoxymethyl)furan-2-carboxylate over Ti-BEA is much slower than over Sn-BEA and Zr-BEA.[20] Unlike Sn-BEA, the active site structure in Ti-BEA is not fully understood, owing to a lack of suitable characterization techniques.[69]

CONCLUSION

We have employed electronic structure calculations and microkinetic modelling to investigate the Diels-Alder aromatization of 2,5-dimethylfuran and ethylene to *p*-xylene over the Lewis-acidic zeotypes Sn-, Zr- and Ti-BEA. We have been motivated by the fact that, while the published experimental work has made it clear that these Lewis acids can catalyze the dehydration of the Diels-Alder product of 2,5-dimethylfuran and ethylene, the kinetic studies have not been able to elucidate whether these same Lewis acids can also catalyze the Diels-Alder step itself.

The present study has shown that there is only minor catalysis of the Diels-Alder, which should be solely attributed to confinement (i.e., entropic) phenomena that vary according to the translational freedom allowed to the species inside the zeolite; the Diels-Alder free energy barriers drop by a modest 1-5 kcal/mol as we increase the translational degrees of freedom of the adsorbates in the pores. However, sensitivity analysis of the MKM-predicted rates shows that the heterogeneous Diels-Alder pathways do not contribute to the overall rate even if we allow for mobile adsorbates in the zeolite. In addition, the same analysis reveals that the rate of *p*-xylene formation is limited by the homogeneous cycloaddition at high acid site concentrations.

Our calculations have also shown that only the partially hydrolyzed ("open") Lewis acid sites are catalytically active and that the silanol group of the open sites is moderately Brønsted acidic and, in fact, catalytically responsible for the hydrolysis of the furan.

Of the three zeotypic Lewis acids tested in this work, Zr-BEA and Sn-BEA have very similar activities, in agreement with experiment, while Ti-BEA is found to be quite inactive, which leads us to suggest that the Ti-BEA catalytic activity recently reported for the formation of *p*-xylene from dimethylfuran and ethylene was likely due to defect sites possessing Brønsted acidity.

ACKNOWLEDGEMENTS

We acknowledge support from the Catalysis Center for Energy Innovation, an Energy Frontier Research Center funded by the U.S. Department of Energy, Office of Science, Office of Basic Energy Sciences under Award number DE-SC0001004. This research used resources of the National Energy

Research Scientific Computing Center (NERSC), a DOE Office of Science User Facility supported by the Office of Science of the U.S. Department of Energy under Contract No. DE-AC02-05CH11231.

TABLES AND FIGURES.

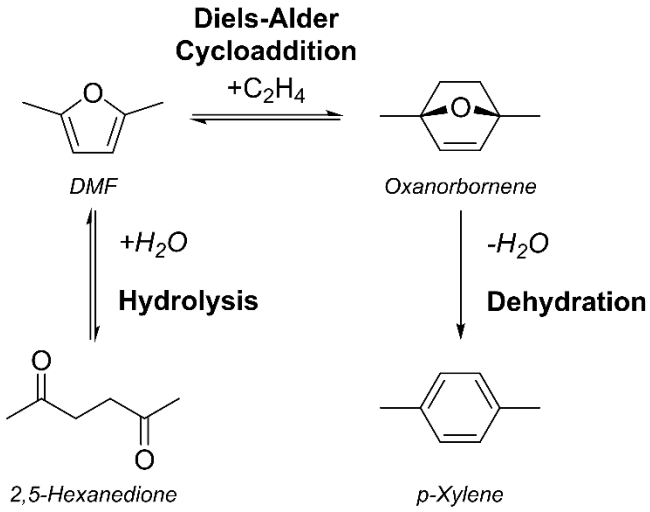

Scheme 1. Diels-Alder aromatization of 2,5-dimethylfuran (DMF) and ethylene to *p*-xylene; and hydrolysis of DMF to 2,5-hexanedione.

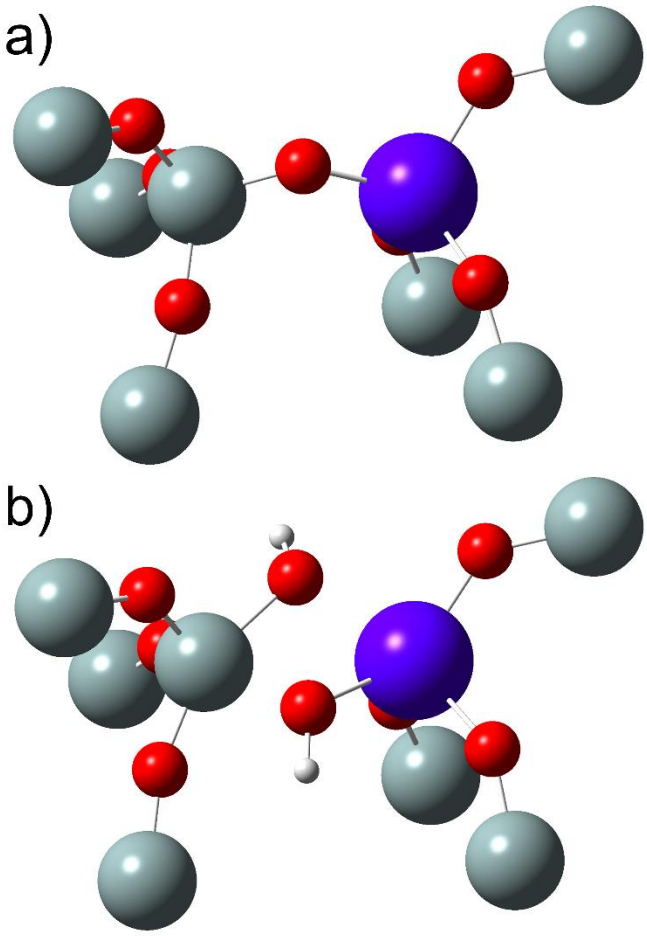

Figure 1. a) "Closed" active site, and b) "open" active site representations of Sn-BEA. Surrounding atoms have been hidden for clarity. (H – white; Si – gray; O – red, Sn – purple).

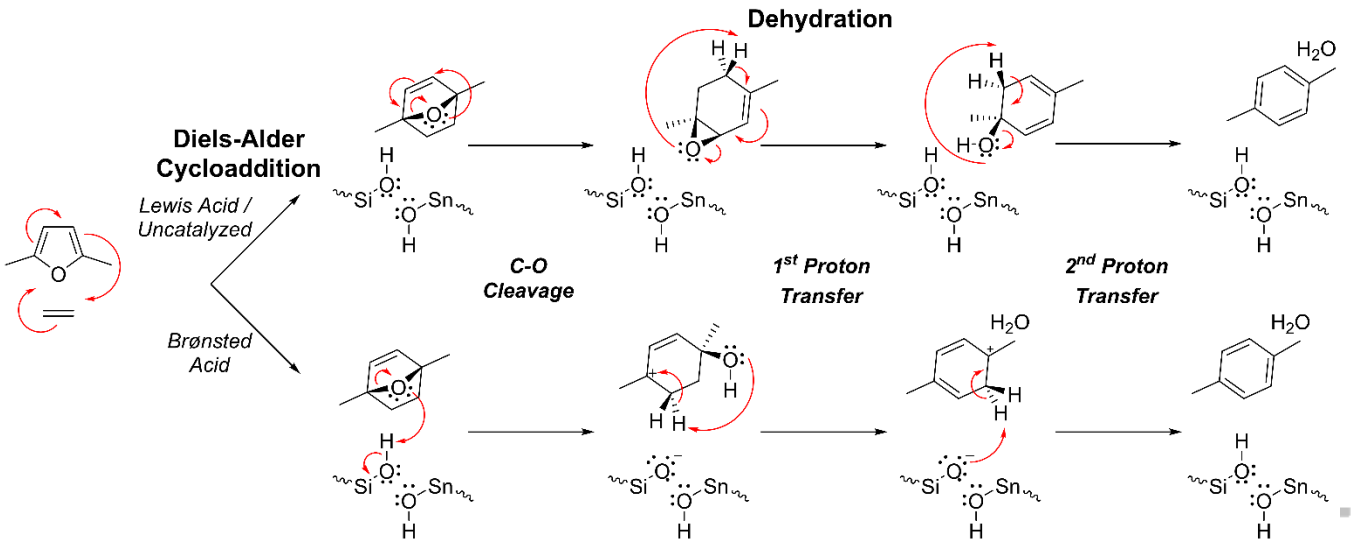

Scheme 2. Reaction mechanism for the Diels-Alder cycloaddition of DMF and ethylene, and subsequent three-step dehydration to water and *p*-xylene. Top mechanism, uncatalyzed or Lewis acid catalysis; bottom maechanism, Brønsted acid catalysis.

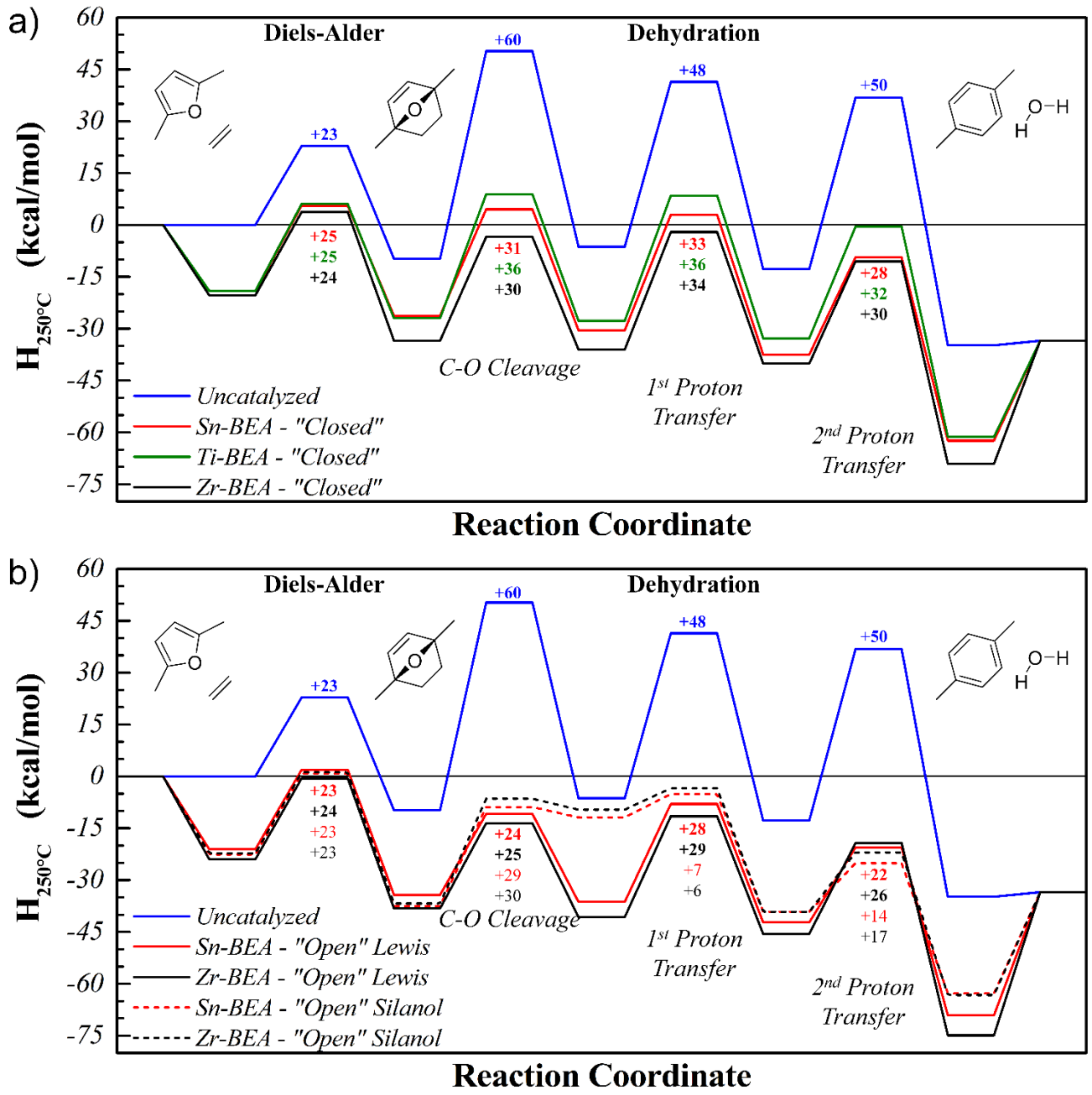

Figure 2. Enthalpy profiles for the Diels-Alder aromatization of DMF and ethylene to p-xylene. a) Unhydrolyzed ("closed") active sites. b) Hydrolyzed ("open") active sites. Values marking transition states indicate intrinsic reaction barriers of corresponding elementary steps and are colored to match the legend. Homogeneous, uncatalyzed reactions calculated at the M06-2X/6-311G(d,p) theory level.

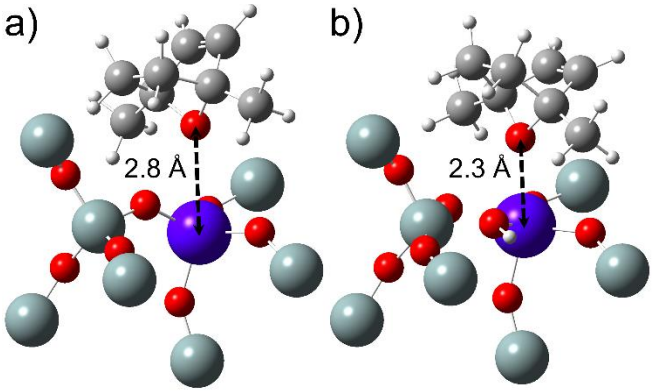

Figure 3. Binding geometries of the Diels-Alder cycloadduct at the Sn-BEA a) "closed" and b) "open" active sites. In both cases coordination is via the bridge O atom of the cycloadduct. Notice the difference in the metal atom-O atom distance, suggesting much stronger interaction of the cycloadduct with the open active site.

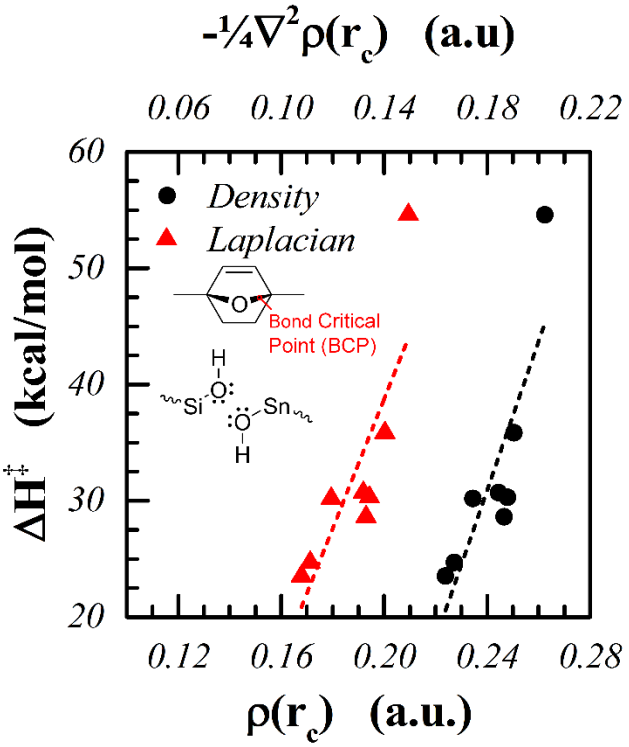

Figure 4. Enthalpy of activation of cycloadduct C-O bridge cleavage plotted against the value of the electron density and the value of the negative of the Laplacian of the electron density at the bond critical point (BCP) of the C-O bond.

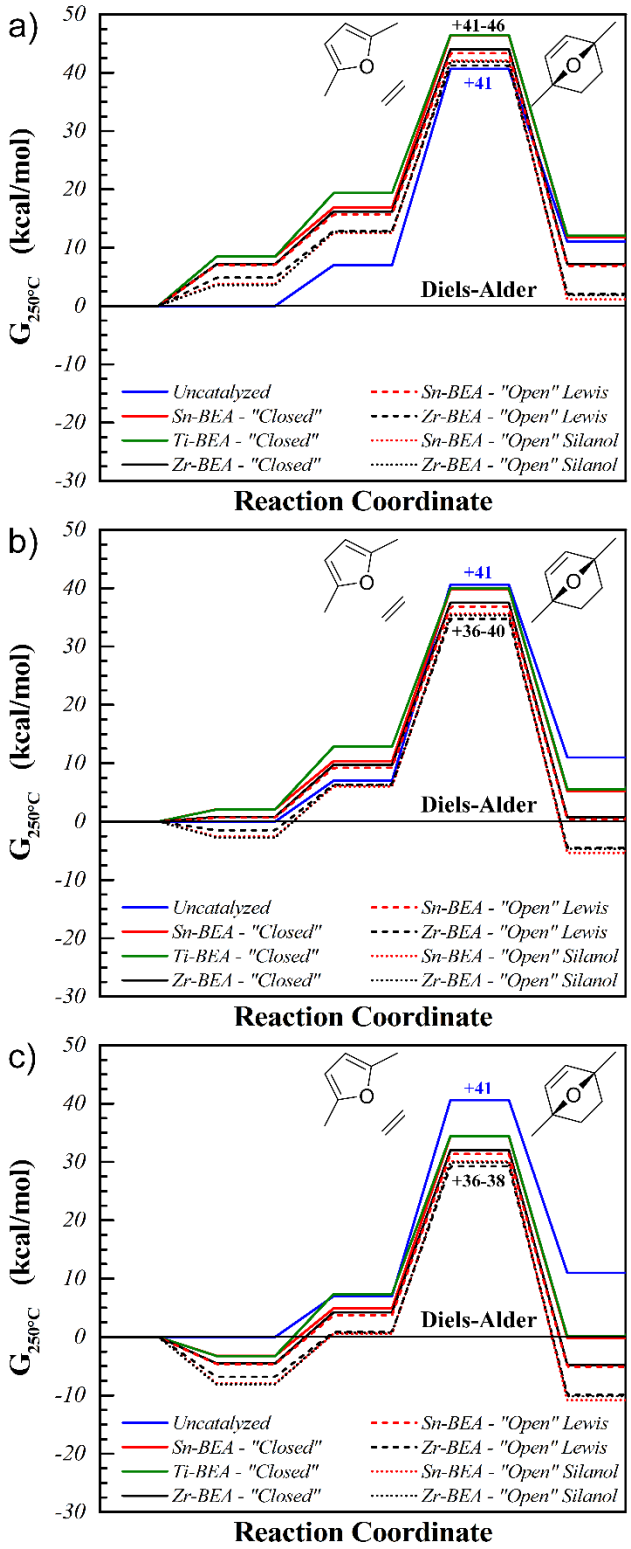

Figure 5. Free energy profiles for the Diels-Alder cycloaddition of DMF and ethylene in different catalysts. a) Immobile adsorbates. b) Mobile adsorbates, free to undergo translational motion in one dimension. c) Mobile adsorbates, free to undergo translational motion in two dimensions. Values marking the transition states indicate free energy barriers with respect to isolated reactants or to adsorbed DMF, whichever lies lower. Homogeneous, uncatalyzed reaction calculated at the M06-2X/6-311G(d,p) theory level.

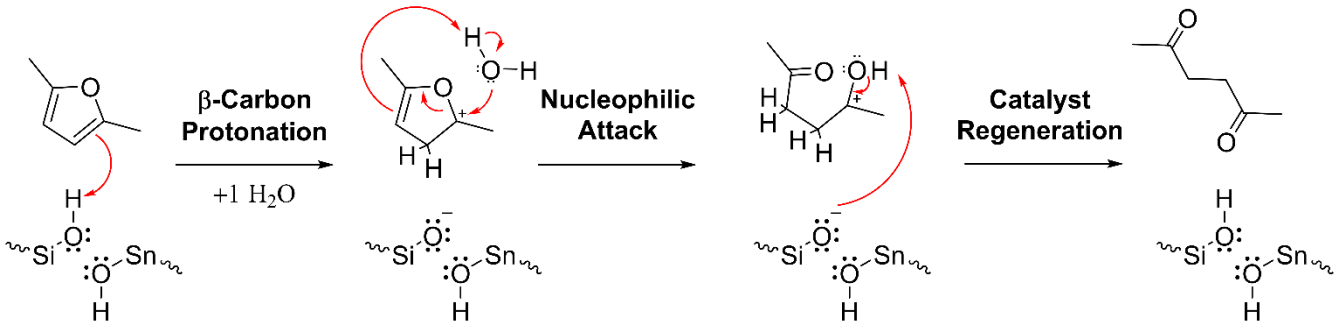

Scheme 3. Reaction mechanism for the hydrolysis of DMF.

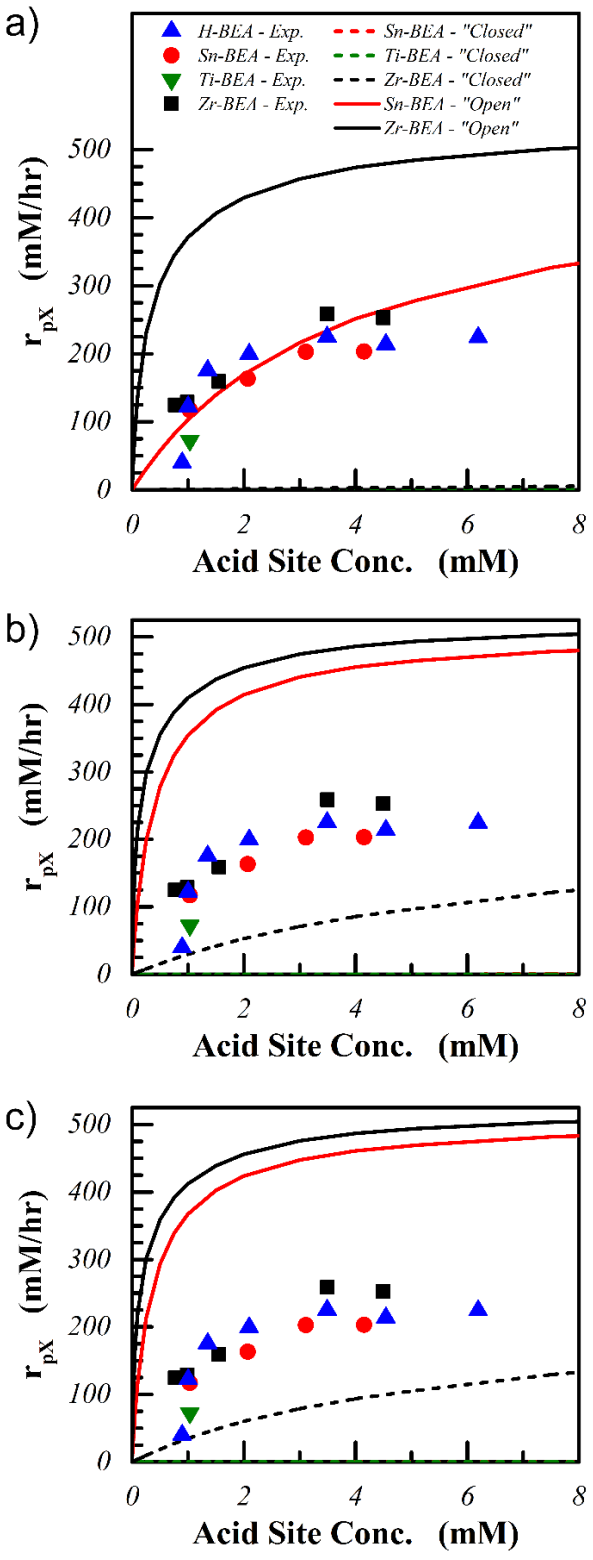

Figure 6. Microkinetic model predicted rates of *p*-xylene production as a function of acid site concentration, using the CBS-QB3 theory level parameterization for the homogeneous Diels-Alder reaction. a) Immobile adsorbates. b) Mobile adsorbates free to undergo translational motion in one dimension. c) Mobile adsorbates free to undergo translational motion in two dimensions. Simulations run at experimental conditions, 250 °C and 37 atm.

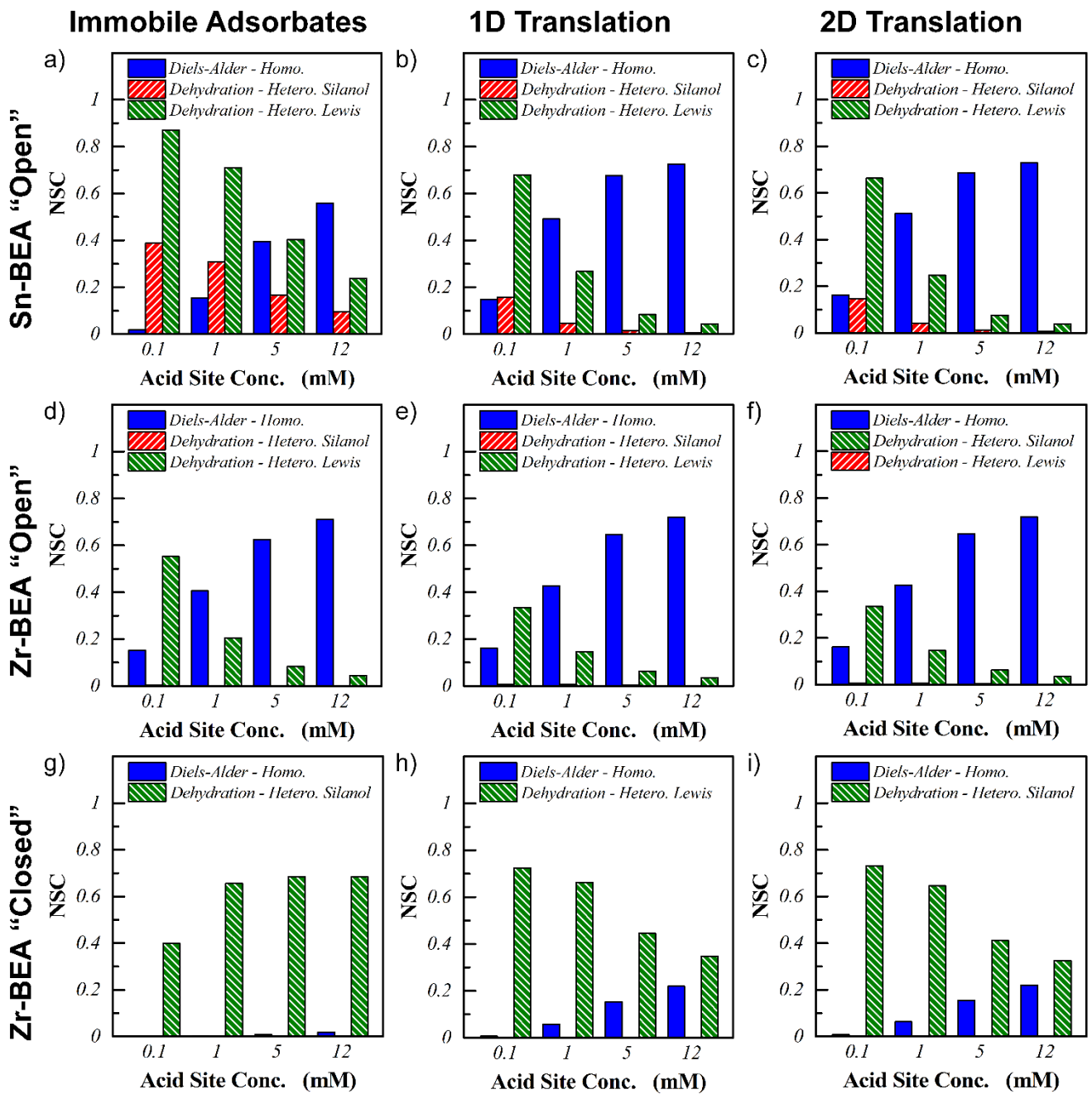

Figure 7. Sensitivity analysis for the formation of *p*-xylene from DMF and ethylene in open-Sn-BEA with a) immobile adsorbates, b) adsorbates with 1D translation in the pores, and c) adsorbates with 2D translation in the pores; open-Zr-BEA with d) immobile adsorbates, e) adsorbates with 1D translation in the pores, and f) adsorbates with 2D translation in the pores; and closed-Zr-BEA with g) immobile adsorbates, h) adsorbates with 1D translation in the pores, and i) adsorbates with 2D translation in the pores. For all systems considered, the heterogeneous Diels-Alder NSC was less than 0.01 and thereby has been omitted from the figures for clarity. The CBS-QB3 theory level parameterization has been used for the kinetics of the homogeneous Diels-Alder reaction.

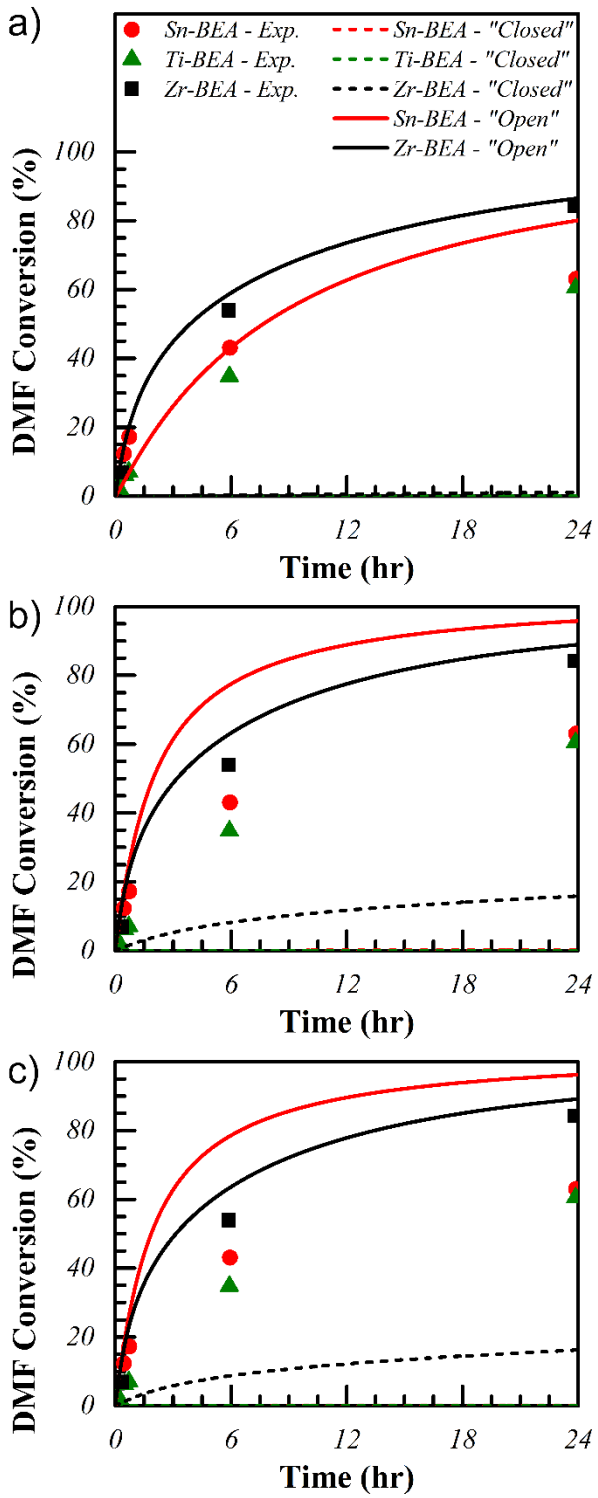

Figure 8. Microkinetic model predicted DMF conversion as a function of time, using the CBS-QB3 theory level parameterization for the homogeneous Diels-Alder reaction. a) Immobile adsorbates. b) Mobile adsorbates free to undergo translational motion in one dimension. c) Mobile adsorbates free to undergo translational motion in two dimensions. Simulations run at experimental conditions, 250 °C and 37 atm.

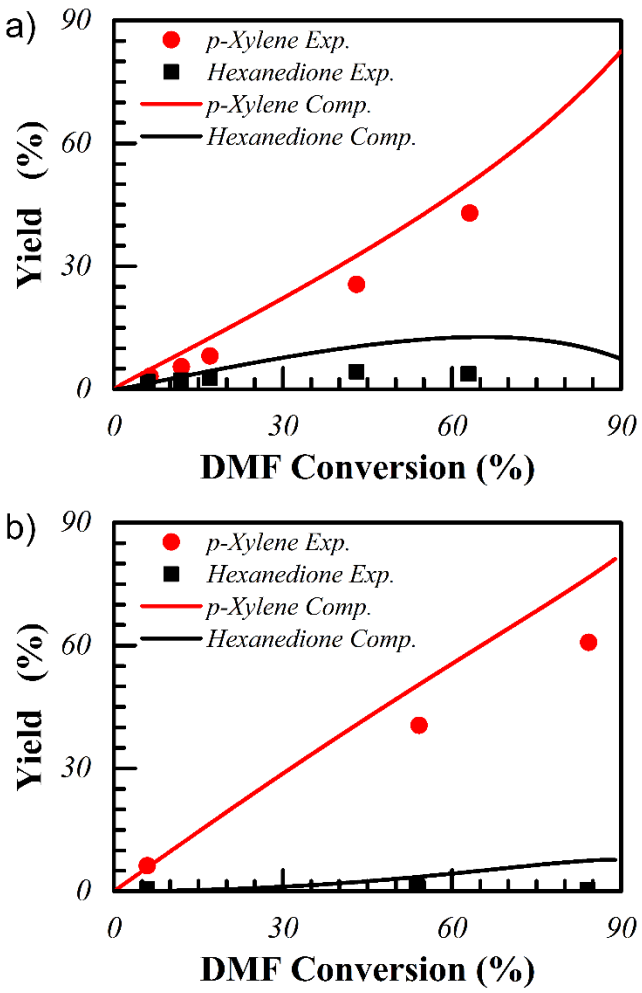

Figure 9. Microkinetic model predicted *p*-xylene (pX) and 2,5-hexanedione (HDI) yields as a function of DMF conversion, using the CBS-QB3 theory level parameterization for the homogeneous Diels-Alder reaction in a) open-Sn-BEA and b) open-Zr-BEA.

Table 1. NBO analysis of Sn-, Ti-, and Zr-BEA closed and open active sites. The Si atom is that which is hydrolyzed into the Si-OH unit of the open site. The O-atom represents the bridging O in the closed site, and the O-atom taken as part of the Si-OH unit of the open site. The H-atom was taken as part of the Si-OH unit of the open site.

	Sn-BEA "Closed"	**Ti-BEA "Closed"**	**Zr-BEA "Closed"**	**Sn-BEA "Open"**	**Zr-BEA "Open"**
Charge – T $(q_T)^a$	2.84	1.95	2.54	2.85	2.53
Charge – Si (q_{Si})	2.57	2.57	2.56	2.50	2.49
Charge – O (q_O)	-1.33	-1.11	-1.25	-1.13	-1.10
Charge – H (q_H)	---	---	---	0.53	0.53
Bond Distance – T-O $(D_{T\text{-}O})^a$ *(Å)*	1.84	1.76	1.91	2.01	2.14
Bond Distance – Si-O $(D_{Si\text{-}O})$ *(Å)*	1.59	1.60	1.59	1.80	1.79
Bond Angle – T-O-Si $(A_{T\text{-}O\text{-}Si})^a$ *(°)*	133.8	137.8	131.8	101.7	99.7
Bond Distance – O-H $(D_{O\text{-}H})$ *(Å)*	---	---	---	0.96	0.96
Deprotonation Energy (kcal/mol)	---	---	---	284.6	298.2

[a] T = Sn, Ti, or Zr

Table 2. Experimental and computed apparent activation energies of the active catalytic systems for immobile adsorbates and for adsorbates allowed to translate freely in one and two dimensions. Microkinetic model run for 15% DMF in 100 mL n-heptane with 200 psi ethylene at 250°C, 550 psi, and for 50 minutes with the indicated catalyst loading.

E_a (kcal/mol)	**Immobile Adsorbates**	**Adsorbates 1D Translation**			**Adsorbates 2D Translation**		
Acid Site Conc. (mM)	**Zr-BEA "Open"**	**Sn-BEA "Open"**	**Zr-BEA "Open"**	**Zr-BEA "Closed"**	**Sn-BEA "Open"**	**Zr-BEA "Open"**	**Zr-BEA "Closed"**
Exp. (0.1 g)	16.3	15.5	16.3	16.3	15.5	16.3	16.3
0.1	13.0	14.8	16.7	19.7	15.2	16.7	20.9
1.0	17.4	18.4	18.4	19.6	18.7	18.5	20.6
5.0	20.2	20.3	20.4	17.4	20.4	20.4	17.6
12.0	20.9	20.7	20.8	16.5	20.7	20.8	16.5

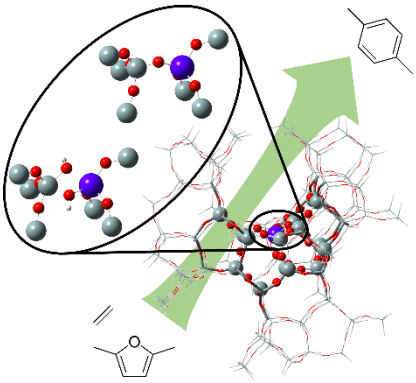

Table of Contents Figure

REFERENCES

1. J. L. Pellegrino, *Energy and Environmental Profile of the U.S. Chemical Industry*, U.S. Department of Energy Office of Industrial Technologies, Columbia MD, **2000**.
2. A. J. Ragauskas, *Science*, **2006**, *311*, 484-489.
3. J. van Haveren, E. L. Scott and J. Sanders, *Biofuels, Bioprod. Biorefin.*, **2008**, 2, 41–57.
4. A. Corma, S. Iborra and A. Velty, *Chem. Rev.*, **2007**, *107*, 2411-2502.
5. J. B. Binder and R. T. Raines, *J. Am. Chem. Soc.*, **2009**, *131*, 1979-1985.
6. D. G. Vlachos, J. G. Chen, R. J. Gorte, G. W. Huber and M. Tsapatsis, *Catal. Lett.*, **2010**, *140*, 77-84.
7. US20100331568 A1, 2010.
8. M. J. Climent, A. Corma and S. Iborra, *Green Chem.*, **2011**, *13*, 520.
9. N. Guo, S. Caratzoulas, D. J. Doren, S. I. Sandler and D. G. Vlachos, *Energy Environ. Sci.*, **2012**, *5*, 6703.
10. R. A. Sheldon, *Green Chem.*, **2014**, *16*, 950-963.
11. P. J. Dauenhauer and G. W. Huber, *Green Chem.*, **2014**, *16*, 382-383.
12. A. Gandini, *Polym. Chem.*, **2010**, *1*, 245-251.
13. Y. Roman-Leshkov, C. J. Barrett, Z. Y. Liu and J. A. Dumesic, *Nature*, **2007**, *447*, 982-985.
14. X. Tong, Y. Ma and Y. Li, *Appl. Catal., A*, **2010**, *385*, 1-13.
15. C. L. Williams, C.-C. Chang, P. Do, N. Nikbin, S. Caratzoulas, D. G. Vlachos, R. F. Lobo, W. Fan and P. J. Dauenhauer, *ACS Catal.*, **2012**, *2*, 935-939.
16. P. T. M. Do, J. R. McAtee, D. A. Watson and R. F. Lobo, *ACS Catal.*, **2013**, *3*, 41-46.
17. C.-C. Chang, S. K. Green, C. L. Williams, P. J. Dauenhauer and W. Fan, *Green Chem.*, **2014**, *16*, 585-588.
18. R. E. Patet, N. Nikbin, C. L. Williams, S. K. Green, C.-C. Chang, W. Fan, S. Caratzoulas, P. J. Dauenhauer and D. G. Vlachos, *ACS Catal.*, **2015**, *5*, 2367-2375.
19. S. K. Green, R. E. Patet, N. Nikbin, C. L. Williams, C.-C. Chang, J. Yu, R. J. Gorte, S. Caratzoulas, W. Fan and D. G. Vlachos, *Appl. Catal., B*, **2016**, *180*, 487-496.
20. J. J. Pacheco and M. E. Davis, *Proc. Natl. Acad. Sci. U.S.A.*, **2014**, *111*, 8363-8367.
21. J. J. Pacheco, J. A. Labinger, A. L. Sessions and M. E. Davis, *ACS Catal.*, **2015**, *5*, 5904-5913.
22. R. A. F. Tomás, J. C. M. Bordado and J. F. P. Gomes, *Chem. Rev.*, **2013**, *113*, 7421-7469.
23. M. Orazov and M. E. Davis, *Chem Sci*, **2016**, *7*, 2264-2274.
24. C.-C. Chang, H. J. Cho, J. Yu, R. J. Gorte, J. Gulbinski, P. Dauenhauer and W. Fan, *Green Chem.*, **2016**, *18*, 1368-1376.
25. N. Nikbin, P. T. Do, S. Caratzoulas, R. F. Lobo, P. J. Dauenhauer and D. G. Vlachos, *J. Catal.*, **2013**, *297*, 35-43.
26. U. Pindur, G. Lutz and C. Otto, *Chem. Rev.*, **1993**, *93*, 741-761.
27. R. B. Woodward and R. Hoffmann, *Angew. Chem. Int. Ed.*, **1969**, *8*, 781-932.
28. K. Fukui, *Acc. Chem. Res.*, **1971**, *4*, 57-64.
29. K. Fukui, *Science*, **1982**, *218*, 747-754.
30. T. L. Gilchrist and R. C. Storr, *Organic Reactions and Orbital Symmetry*, Cambridge University Press, New York, Second edn., **1979**.
31. K. N. Houk, *J. Am. Chem. Soc.*, **1973**, *95*, 4092-4094.
32. K. N. Houk and R. W. Strozier, *J. Am. Chem. Soc.*, **1973**, *95*, 4094-4096.
33. K. N. Houk, *Acc. Chem. Res.*, **1975**, *8*, 361-369.

34. P. Geerlings, F. De Proft and W. Langenaeker, *Chem. Rev.*, **2003**, *103*, 1793-1874.
35. L. R. Domingo, P. Perez and R. Contreras, *Tetrahedron*, **2004**, *60*, 6585-6591.
36. L. R. Domingo, M. J. Aurell, P. Perez and R. Contreras, *Tetrahedron*, **2002**, *58*, 4417-4423.
37. L. R. Domingo, M. J. Aurell, P. Perez and R. Contreras, *J. Phys. Chem. A*, **2002**, *106*, 6871-6875.
38. L. R. Domingo, A. Asensio and P. Arroyo, *J. Phys. Org. Chem.*, **2002**, *15*, 660-666.
39. L. R. Domingo, *Eur. J. Org. Chem.*, **2004**, *2004*, 4788-4793.
40. L. R. Domingo, *Tetrahedron*, **2002**, *58*, 3765-3774.
41. L. R. Domingo, M. Arnó and J. Andrés, *J. Org. Chem.*, **1999**, *64*, 5867-5875.
42. L. R. Domingo and J. A. Sáez, *Org. Biomol. Chem.*, **2009**, *7*, 3576-3583.
43. N. Nikbin, S. Feng, S. Caratzoulas and D. G. Vlachos, *J. Phys. Chem. C*, **2014**, *118*, 24415-24424.
44. R. Braun and J. Sauer, *Eur. J. Inorg. Chem.*, **1986**, *119*, 1269-1274.
45. P. K. Chattaraj, U. Sarkar and D. R. Roy, *Chem. Rev.*, **2006**, *106*, 2065-2091.
46. V. Eschenbrenner-Lux, P. Z. Kuchler, S., K. Kumar and H. Waldmann, *Angew. Chem. Int. Ed.*, **2014**, *53*, 2134−2137.
47. T. Salavati-fard, S. Caratzoulas and D. J. Doren, *J. Phys. Chem. A*, **2015**, *119*, 9834-9843.
48. M. Svensson, S. Humbel, R. D. J. Froese, T. Matsubara, S. Sieber and K. Morokuma, *J. Phys. Chem.*, **1996**, *100*, 19357-19363.
49. S. Dapprich, I. Komáromi, K. S. Byun, K. Morokuma and M. J. Frisch, *J. Mol. Struct.*, **1999**, *461*, 1-21.
50. L. W. Chung, W. M. C. Sameera, R. Ramozzi, A. J. Page, M. Hatanaka, G. P. Petrova, T. V. Harris, X. Li, Z. Ke, F. Liu, H.-B. Li, L. Ding and K. Morokuma, *Chem. Rev.*, **2015**, *115*, 5678-5796.
51. C. Baerlocher and L. B. McCusker, *International Zeolite Association*, **1996**.
52. Y. Zhao and D. G. Truhlar, *Theor. Chem. Acc.*, **2008**, *120*, 215-241.
53. A. K. Rappé, C. J. Casewit, K. Colwell, W. Goddard Iii and W. Skiff, *J. Am. Chem. Soc.*, **1992**, *114*, 10024-10035.
54. R. Bermejo-Deval, M. Orazov, R. Gounder, S. J. Hwang and M. E. Davis, *ACS Catal.*, **2014**, *4*, 2288-2297.
55. T. Blasco, M. A. Camblor, A. Corma, P. Esteve, J. M. Guil, A. Martínez, J. A. Perdigón-Melón and S. Valencia, *J. Phys. Chem. B*, **1998**, *102*, 75-88.
56. A. V. Marenich, C. J. Cramer and D. G. Truhlar, *J. Phys. Chem. B*, **2009**, *113*, 6378-6396.
57. Gaussian 09, M. J. Frisch, G. W. Trucks, H. B. Schlegel, G. E. Scuseria, M. A. Robb, J. R. Cheeseman, G. Scalmani, V. Barone, B. Mennucci, G. A. Petersson, H. Nakatsuji, M. Caricato, X. Li, H. P. Hratchian, A. F. Izmaylov, J. Bloino, G. Zheng, J. L. Sonnenberg, M. Hada, M. Ehara, K. Toyota, R. Fukuda, J. Hasegawa, M. Ishida, T. Nakajima, Y. Honda, O. Kitao, H. Nakai, T. Vreven, J. A. Montgomery Jr., J. E. Peralta, F. Ogliaro, M. J. Bearpark, J. Heyd, E. N. Brothers, K. N. Kudin, V. N. Staroverov, R. Kobayashi, J. Normand, K. Raghavachari, A. P. Rendell, J. C. Burant, S. S. Iyengar, J. Tomasi, M. Cossi, N. Rega, N. J. Millam, M. Klene, J. E. Knox, J. B. Cross, V. Bakken, C. Adamo, J. Jaramillo, R. Gomperts, R. E. Stratmann, O. Yazyev, A. J. Austin, R. Cammi, C. Pomelli, J. W. Ochterski, R. L. Martin, K. Morokuma, V. G. Zakrzewski, G. A. Voth, P. Salvador, J. J. Dannenberg, S.

Dapprich, A. D. Daniels, Ö. Farkas, J. B. Foresman, J. V. Ortiz, J. Cioslowski and D. J. Fox, Gaussian, Inc., Wallingford CT, **2009**.
58. S. Grimme, *Chem. Eur. J.*, **2012**, *18*, 9955-9964.
59. Y.-P. Li, J. Gomes, S. M. Sharada, A. T. Bell and M. Head-Gordon, *J. Phys. Chem. C*, **2015**, *119*, 1840-1850.
60. R. E. Patet, S. Caratzoulas and D. G. Vlachos, *Phys. Chem. Chem. Phys.*, **2016**, *18*, 26094-26106.
61. E. D. Glendening, C. R. Landis and F. Weinhold, *J. Comput. Chem.*, **2013**, *34*, 1429-1437.
62. R. F. Bader, *Chem. Rev.*, **1991**, *91*, 893–928.
63. B. A. De Moor, M.-F. Reyniers, O. C. Gobin, J. A. Lercher and G. B. Marin, *J. Phys. Chem. C*, **2011**, *115*, 1204-1219.
64. S. Kozuch and S. Shaik, *J. Am. Chem. Soc.*, **2006**, *128*, 3355-3365.
65. S. Kozuch and S. Shaik, *Acc. Chem. Res.*, **2011**, *44*, 101-110.
66. S. Kozuch and J. M. L. Martin, *ACS Catal.*, **2012**, 2, 2787-2794.
67. J. Yu, S. Zhu, P. J. Dauenhauer, H. J. Cho, W. Fan and R. Gorte, *Catal. Sci. Technol.*, **2016**, *6*, 5729-5736.
68. N. Nikbin, S. Caratzoulas and D. G. Vlachos, *ChemSusChem*, **2013**, *6*, 2066-2068.
69. S. Pei, G. W. Zajac, J. A. Kaduk, J. Faber, B. I. Boyanov, D. Duck, D. Fazzini, T. I. Morrison and D. S. Yang, *Catal. Lett.*, **1993**, *21*, 333-344.